Multiple scattering formulation of two-dimensional acoustic and electromagnetic metamaterials

2011 New J. Phys. 13 093018

(http://iopscience.iop.org/1367-2630/13/9/093018)

New Journal of Physics
The open-access journal for physics

Multiple scattering formulation of two-dimensional acoustic and electromagnetic metamaterials

Daniel Torrent[1] **and José Sánchez-Dehesa**[1]

Grupo de Fenómenos Ondulatorios, Departamento de Ingeniería Electrónica, Universitat Politècnica de València, Camino de Vera s/n (Edificio 7F), ES-46022 Valencia, Spain
E-mail: datorma1@upvnet.upv.es and jsdehesa@upvnet.upv.es

New Journal of Physics **13** (2011) 093018 (25pp)
Received 18 January 2011
Published 9 September 2011
Online at http://www.njp.org/
doi:10.1088/1367-2630/13/9/093018

Abstract. A multiple scattering formulation of two-dimensional (2D) acoustic metamaterials is presented. This approach is comprehensive and can lead to frequency-dependent effective parameters (scalar bulk modulus and tensorial mass density), as it is possible to have not only positive or negative ellipsoidal refractive index, but also positive or negative hyperbolic refractive index. The correction due to multiple scattering interactions is included in the theory and it is demonstrated that its contribution is important only for lattices with high filling fractions. Since the surface fields on the scatterers are mainly responsible for the anomalous behavior of the resulting effective medium, complex scatterers can be used to engineer the frequency response. Anisotropic effects are also discussed within this formulation and some numerical examples are reported. A homogenization theory is also extended to electromagnetic wave propagation in 2D lattices of dielectric structures, where Mie resonances are found to be responsible for the metamaterial behavior.

[1] Authors to whom any correspondence should be addressed.

Contents

1. Introduction

Fluid-like metamaterials or metafluids with negative constitutive parameters offer new insights into acoustic wave propagation. Single negative metamaterials (SNM), in which either the mass density or the bulk modulus is negative [1–3], can be used, for example, for the fabrication of surface-like acoustic lens to overcome the diffraction limit [4, 5] or acoustic panels that attenuate low-frequency noise [6]. Double-negative metamaterials (DNM) [7–9] exhibit negative refraction [10–13] and, as is well known from electromagnetic (EM) wave theory, they can also be used to increase the resolution of conventional lens [14–16]. In general, anisotropic fluid-like metamaterials with acoustic parameters, both positive and negative are necessary, in the field of transformation acoustics for designing different types of acoustic devices [17–21].

The existence of frequency ranges where the effective medium presents negative constitutive parameters is related to subwavelength resonances of the individual scatterers that constitute the metamaterial. These resonances can be, for example, due to soft-scatterer resonances [7, 22, 23] or to Helmholtz-like resonances [2, 8], [24–26]. The same phenomenon is found in EM waves under the name of Mie resonances [27–31], and they present an alternative way of designing EM metamaterials to that offered by split ring resonators [32] or metallodielectric composites [13, 33, 34], which have been the dominant structures so far. Therefore, metamaterials based on local resonances are important not only for acoustic but also for EM metamaterials.

It is known that the monopolar resonances in the individual scatterers are responsible for negative bulk modulus and that the dipolar ones are responsible for negative mass density [7, 35]. However, the behavior of aggregates of scatterers in the homogenization limit has been partially explained since multiple scattering effects or anisotropic lattices have not been studied in depth.

Here, we give a description of acoustic metamaterials by using a multiple scattering approach under the assumption that the wavelength in the background is asymptotically large,

whereas inside the scatterer, it remains finite. It is based on our theory already applied to the homogenization of sonic crystals [36–38]. We consider in the long-wavelength limit an ensemble of ordered or disordered scatterers as an effective medium with acoustic parameters that are frequency dependent and can take negative values in certain frequency regions. The frequency-dependent parameters are given in terms of the lattice symmetry, the multiple scattering interactions and the fields at the scatterers' surface. This formulation recovers all the previous results regarding SNM and DNM and, moreover, can be applied to any type of radially symmetric scatterer, to non-symmetric lattices and even to any filling fraction.

This paper is organized as follows. In section 2, the concept of low-frequency resonances is introduced, showing how these resonances lead to scatterers with locally negative parameters. Section 3 describes the multiple scattering formulation and reports its application to the case of lattices with low filling fraction as well as to the more general case, showing how anisotropy appears. In this section, the theory is extended to include multipolar effects, but we see that they are important for high filling fractions and for high acoustic contrast. Also, it is shown that the multiple scattering corrections are independent of frequency. In section 4, the application of the theory to EM waves is explained in brief. The paper ends with a summary in section 5 and two appendices. Appendix A analyzes several examples of scatterers with locally negative parameters showing that tuning the scatterers' resonances can be achieved using complex scatterers, whereas appendix B gives the technical details of the derivation of the frequency-dependent Δ factor, which is responsible for the multiple scattering effects in the homogenization theory.

2. Low-frequency resonances and locally negative parameters

Homogenization theories for aggregates of scatterers are based on small-wavenumber (long-wavelength) expansions of the fields in both the background and the scatterers. When working with metamaterials we assume that the wavenumber in the background is asymptotically small although we let the wavenumber inside the scatterer still be finite. Physically it means that outside the scatterers the wave field propagates through an effective medium, but the scatterers are still allowed to have complex scattering processes. The complexity leads to negative parameters in a narrow frequency region, as will be explained below.

A simple example of this type of scatterer (see appendix A) is a homogeneous fluid-like scatterer. If the sound speed inside this scatterer is much smaller than that of the background, $c_a \ll c_b$, we will have that, for a given frequency ω, the wavelength inside the scatterer, λ_a, is also much smaller than that in the background, i.e. $\lambda_a \ll \lambda_b$. Thus, outside the scatterer the field will be a function of $k_b = \omega/c_b$, which is a slowly oscillating function, while inside the scatterer the field will be a rapidly oscillating function of $k_a = \omega/c_a$. Since we are in the low-frequency limit we expect, in principle, the medium to behave as an effective homogeneous medium with constant parameters, but in fact, due to the fields inside the scatterer, the resulting effective medium has parameters that are frequency dependent.

The next subsection analyzes this effect rigorously and appendix A includes the results for different types of scatterers, showing how complex scatterers present frequency-dependent behavior. The latter, as will be seen in section 3, can lead to metamaterials with negative constitutive parameters.

2.1. Acoustic scatterers with locally negative parameters

The wave equation for a pressure field in an inhomogeneous fluid is given as [39]

$$\nabla\left[\rho^{-1}(\boldsymbol{r})\nabla P(\boldsymbol{r})\right]+\frac{\omega^2}{B(\boldsymbol{r})}P(\boldsymbol{r})=0, \tag{1}$$

where $\rho(\boldsymbol{r})$ and $B(\boldsymbol{r})$ are the fluid mass density and bulk modulus, respectively, and $\boldsymbol{r}=(r,\theta)$ defines an arbitrary point in the x–y-plane in polar coordinates. We also consider that the scatterer, which has radius R_a and is radially symmetric with parameters $\rho(r)$ and $B(r)$, is embedded into a fluid background with acoustic parameters ρ_b and B_b.

This is a canonical problem whose solution outside the scatterer is given in terms of the Bessel and Hankel functions [39],

$$P(r,\theta;\omega)=\sum_{q=-\infty}^{\infty}A_q^0\left[J_q(k_br)+T_qH_q(k_br)\right]\mathrm{e}^{\mathrm{i}q\theta},\quad r>R_a \tag{2}$$

with $k_b^2=\omega^2\rho_b/B_b$. The coefficients A_q^0 are determined by the incident field, and the scatterer response is described by the matrix elements T_q. This matrix is diagonal for the case considered due to axial symmetry of the scatterer, and it can be obtained by solving the wave equation (1) inside the scatterer and applying boundary conditions at the scatterer surface, $r=R_a$. The conditions are the continuity of the pressure field and the normal component of the velocity,

$$P(R_a^+)=P(R_a^-), \tag{3a}$$

$$\frac{1}{\rho_b}\partial_rP(R_a^+)=\frac{1}{\rho(R_a^-)}\partial_rP(R_a^-). \tag{3b}$$

Since the scatterer is radially symmetric and parameters ρ and B depend only on the radial coordinate, the field inside the scatterer can be expressed as a Fourier series of the form

$$P(r,\theta;\omega)=\sum_{q=-\infty}^{\infty}B_q(\omega)\psi_q(r;\omega)\mathrm{e}^{\mathrm{i}q\theta}, \tag{4}$$

where the eigenfunctions $\psi_q(r;\omega)$ are the solutions of the radial part of equation (1) in cylindrical coordinates,

$$\frac{\rho(r)}{r}\partial_r\left(\frac{r}{\rho(r)}\partial_r\psi_q(r;\omega)\right)+\left(\omega^2\frac{\rho(r)}{B(r)}-\frac{q^2}{r^2}\right)\psi_q(r;\omega)=0. \tag{5}$$

From this equation, after applying the boundary conditions, the general expression for the diagonal components of the T matrix is easily obtained:

$$T_q=-\frac{\chi_qJ_q'(k_bR_a)-J_q(k_bR_a)}{\chi_qH_q'(k_bR_a)-H_q(k_bR_a)},\qquad \chi_q=\frac{\rho(R_a)}{\rho_b}\frac{\psi_q(R_a;\omega)}{\partial_r\psi_q(R_a;\omega)}k_b. \tag{6}$$

This matrix contains two contributions: the background contribution is described by the Bessel and Hankel functions, while the scatterer contribution is described by the function χ_q. In general, equation (5) must be solved in order to obtain the χ_q functions; for example, for a homogeneous and isotropic cylinder of mass density ρ_a and speed of sound c_a, the solutions to equation (5) are Bessel functions; thus

$$\chi_q=\frac{\rho_ac_a}{\rho_bc_b}\frac{J_q(k_aR_a)}{J_q'(k_aR_a)}. \tag{7}$$

Standard homogenization theory based on multiple scattering uses the asymptotic form of these expressions to derive the effective medium properties. In particular, the monopolar and dipolar terms ($q = 0$ and $q = 1$) are used to obtain the effective modulus and mass density, respectively, both being positive [36, 37]. However, it is shown below that metamaterial behavior (i.e. effective parameters with negative values) appears in the regime where only the Bessel and Hankel functions of the background are replaced by their asymptotic forms at low frequencies. In other words, when the wavelength in the background is large, the wavelength in the scatterer is comparable in size.

So, let us then consider that the arguments of the Bessel and Hankel functions are small, $k_b R_a \ll 1$, and use their asymptotic forms [40]. Then, the monopolar component of the T matrix becomes

$$T_0 \approx \frac{\mathrm{i}\pi R_a^2 k_b^2}{4} \frac{1 + \frac{1}{2} k_b R_a \chi_0}{\frac{k_b^2 R_a^2}{2} \ln k_b R_a - \frac{1}{2} k_b R_a \chi_0}, \tag{8}$$

where the logarithmic term in the denominator is negligible in comparison with the linear term in k_b in the low-frequency limit but cannot be neglected when dealing with metamaterials. This term, which has been omitted in many preceding studies about acoustic and EM metamaterials, is of paramount importance to determine the metamaterial effective parameters.

Equivalently, the dipolar component of the T matrix is

$$T_1 \approx \frac{\mathrm{i}\pi R_a^2 k_b^2}{4} \frac{\chi_1 / k_b R_a - 1}{\chi_1 / k_b R_a + 1}. \tag{9}$$

Since we expect similar behavior to that of a homogeneous scatterer with effective acoustic parameters ρ_a and B_a, the matrix elements should have the standard form

$$T_0 \approx \frac{\mathrm{i}\pi R_a^2 k_b^2}{4} \left[\frac{B_b}{B_a} - 1 \right], \tag{10a}$$

$$T_1 \approx \frac{\mathrm{i}\pi R_a^2}{4} \frac{\rho_a - \rho_b}{\rho_a + \rho_b} k_b^2. \tag{10b}$$

Now, comparing equations (8) and (9) with equations (10*a*) and (10*b*), one can introduce frequency-dependent bulk modulus and mass density functions as follows:

$$B_a(\omega)/B_b = \frac{k_b^2 R_a^2}{2} \ln k_b R_a - \frac{1}{2} k_b R_a \chi_0 \tag{11a}$$

$$\rho_a(\omega)/\rho_b = \chi_1 / k_b R_a. \tag{11b}$$

These functions depend on the mass density at the scatterer surface, $\rho(r = R_a)$, and also depend on the field and its derivative at the surface: that is, $\psi_q(r = R_a; \omega)$ and $\partial_r \psi_q(r = R_a; \omega)$, respectively. These quantities are frequency dependent and are responsible for the frequency dependence of the parameters $B_a(\omega)$ and $\rho_a(\omega)$. It is worthwhile to show that $B_a(\omega) \equiv B_b$ and $\rho_a(\omega) \equiv \rho_b$ for a homogeneous scatterer. This is done in appendix A.

The derivation described above is similar to that in [7, 35] where the authors employed the coherent potential approximation method and seek the self-consistent solution to ensure that the inhomogeneous system embedded within an effective medium generates no scattering in the lowest order of frequency. However, in [7, 35] the expressions are left as functions of the so-called scattering coefficients and therefore they are very general and valid for any type

of isotropic scatterer. Here, we gave a further step and analyze the low-frequency limit of the scattering coefficients under the assumption that only the wavenumber in the background is asymptotically large, which allows us to understand metamaterial phenomena.

Appendix A.1 reports several applications of formulae developed above. In particular, three different scatterers with negative acoustic parameters at narrow frequency regions are briefly analyzed.

3. Multiple scattering of acoustic waves in the low-frequency limit

A cluster of cylindrical scatterers defined by their homogeneous parameters ρ_a and B_a will behave in the low-frequency limit (i.e. for wavelengths larger than the typical separation between scatterers) as a homogeneous medium with effective parameters ρ^* and B^*. These parameters were obtained by Berryman [41] in 1980 by making a comparison of the scattering properties of the cluster and the effective scatterer. The resulting estimate was not exact because multiple scattering effects were neglected. This approach was recently generalized by including all the multiple scattering interactions between scatterers and very general expressions were obtained in [36–38].

The following subsections present a generalization of the results of previous studies to the case of metamaterials in which effective parameters are frequency dependent. It will be considered that parameters ρ_a and B_a can be replaced by their corresponding frequency-dependent values $\rho_a(\omega)$ and $B_a(\omega)$. It is demonstrated that this procedure is self-consistent and therefore gives a correct method for the extraction of the effective parameters of acoustic metamaterials.

3.1. Multiple scattering effects: the Δ factor

Let us consider a cluster of scatterers periodically distributed in a fluid background. In the low-frequency limit, the cluster behaves like an effective fluid-like medium with the parameters given as [41]

$$\frac{1}{B^*(\omega)} = \frac{1-f}{B_b} + \frac{f}{B_a(\omega)}, \tag{12a}$$

$$\rho^*(\omega) = \frac{\rho_a(\omega)(1+f) + \rho_b(1-f)}{\rho_a(\omega)(1-f) + \rho_b(1+f)}\rho_b, \tag{12b}$$

where the frequency dependence of scatterer parameters (see equations (11*a*) and (11*b*)) has been included.

While equation (12*a*) is valid for all filling fractions, equation (12*b*) is valid for diluted clusters only (i.e. low filling fractions). In [37] and [38], the expressions for the effective density were generalized to the case of high filling fractions, and all the multiple scattering terms were introduced in equation (12*b*) by means of the so-called Δ factor, leading to

$$\rho^*(\omega) = \frac{\rho_a(\omega)(\Delta+f) + \rho_b(\Delta-f)}{\rho_a(\omega)(\Delta-f) + \rho_b(\Delta+f)}\rho_b. \tag{13}$$

The factor Δ represents a correction to the effective density and takes into account all the multiple scattering interactions between the cylinders in a cluster or in an infinite lattice. Technical details of its derivation are given in appendix B. Δ also contains information on

the mass density of the cylinders forming the cluster and, hence, if we want to introduce a frequency-dependent factor $\Delta(\omega)$, the frequency-dependent mass density must also be considered.

We have shown that the contribution of the scatterers' density to the Δ factor is made through the factor η defined as [37, 38]

$$\eta = \frac{\rho_a - \rho_b}{\rho_a + \rho_b}. \tag{14}$$

It is tempting to replace $\rho_a \to \rho_a(\omega)$ in order to define the frequency-dependent $\Delta(\omega)$. However, it must be remembered that the η factor appears in the power expansion of the q-component of the T matrix as follows:

$$\lim_{k_b \to 0} \frac{T_q}{k_b^{2|q|}} = \frac{\mathrm{i}\pi R_a^{2q}}{q!(q-1)!2^{2q}} \frac{\rho_a - \rho_b}{\rho_a + \rho_b}. \tag{15}$$

Then, for the Δ factor to be consistent with our theory, we must compute T_q given by equation (6) taking into account that the wavelength inside the scatterer is still finite. This leads to the following equation that replaces equation (15):

$$\frac{T_q}{k_b^{2|q|}} \approx \frac{\mathrm{i}\pi R_a^{2q}}{q!(q-1)!2^{2q}} \frac{q\chi_q/k_b R_a - \rho_b}{q\chi_q/k_b R_a + \rho_b}. \tag{16}$$

This equation shows that we can generalize the Δ factor as long as we make the substitution

$$\eta \to \eta(\omega) = \frac{q\chi_q/k_b R_a - \rho_b}{q\chi_q/k_b R_a + \rho_b} \tag{17}$$

in the corresponding multipolar components in [37] and [38].

The Δ factor was studied in the quasi-static limit (i.e. for $\lambda \to \infty$) and it was demonstrated that its contribution is important only for high filling fractions and for strong scatterers [37, 38]. This is because the coupling to higher multipolar components is always weaker. Similar behavior is expected for the frequency-dependent factor, $\Delta(\omega)$, although we would expect in this case the presence of resonances different from monopolar or dipolar. However, it was shown in [38] that the multipolar contributions to the Δ factor are proportional to a set of lattice sums S_q, whose values depend on the lattice symmetry. Thus, for the square or hexagonal lattices only the sums such that $q = 4n$ or $q = 6n$, respectively, for $n = 1, 2, \ldots$, are different from zero. Thus, the first multipolar term appearing in the Δ factor is that with $q = 4$ for a square lattice and with $q = 6$ for a hexagonal one. The resonances of these modes for a lattice of homogeneous cylinders occur at frequencies higher than those for $q = 0$ and $q = 1$. Thus, they cannot be observed in the low-frequency limit. It does not mean, however, that the Δ factor is not relevant, as will be discussed in the following example, but rather that the higher-order resonances do not contribute to the effective parameters.

The contribution of the Δ factor to the effective parameters is better understood for strong scatterers. For the case of almost rigid scatterers (i.e. cylinders made of heavy solid materials embedded in air) this factor contributes considerably to the calculation of the effective parameters, but since these cylinders do not possesses low-frequency internal resonances, they are of no interest to this study. In contrast, the case of soft scatterers like, for example, air cylinders embedded in water represents the opposite system and is discussed below.

Figure 1 shows the bulk modulus of a hexagonal lattice of air cylinders in a water background ($B_a = 5.14 \times 10^{-5} B_b$, $\rho_a = 10^3\,\mathrm{kg\,m^{-3}}$ and $\rho_b = 1.24\,\mathrm{kg\,m^{-3}}$) for several filling

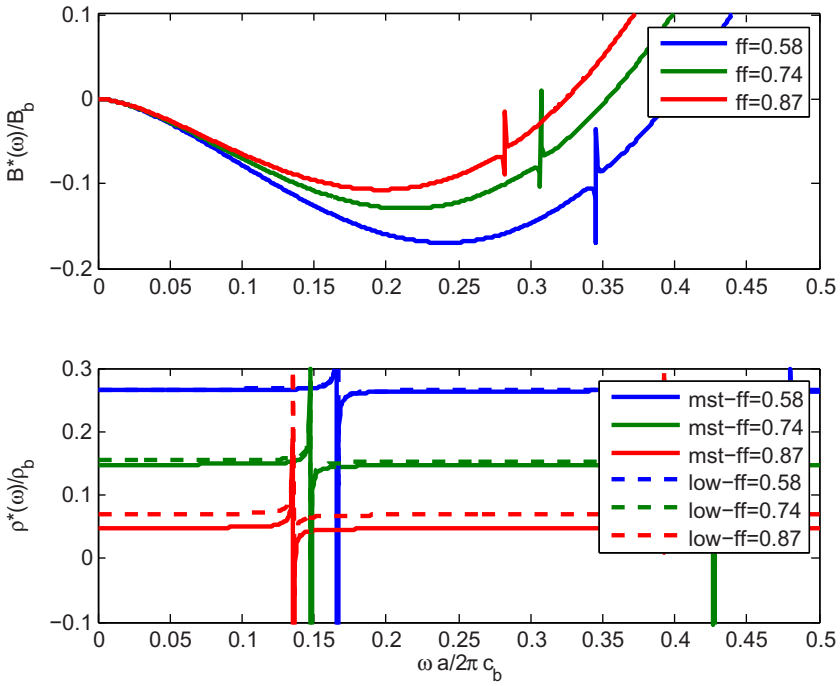

Figure 1. Upper panel: effective bulk modulus of a composite medium made of air cylinders distributed in a hexagonal lattice and embedded in water. The results are shown for three filling fractions ff. The effective bulk modulus is negative in the whole frequency region considered as homogenization. Only in a very narrow region corresponding to infinite wavelength is the effective bulk modulus positive. Lower panel: the corresponding effective mass densities. The dashed lines correspond to the dilute approximation (low-ff) and the continuous lines represent calculations where the multiple scattering terms are considered (mst-ff).

fractions. It has been pointed out that the effective bulk modulus does not need a multiple scattering correction. However, this example demonstrates that the homogenization limit can be defined here only from a frequency-dependent theory since the modulus is negative in a wide frequency range. The expression for the frequency-dependent bulk modulus is given by equation (A.1a), where we observe that, since $B_a/B_b \approx 5 \times 10^{-5}$, the dominant contribution comes from the logarithmic term. The second term contributes to a weak resonance near the reduced frequency of 0.3, as can be observed in the figure. On the one hand, this resonance is too sharp to be measured in a real system; on the other, it occurs beyond what we could consider the homogenization limit, which is found to be at $a/\lambda \approx 0.25$.

The lower panel of figure 1 shows the frequency-dependent mass density for three different filling fractions. The continuous line corresponds to the calculation considering the $\Delta(\omega)$ factor as explained above; the dashed line corresponds to the low filling fraction approximation. It is shown how the multiple scattering correction is important for high filling fractions only, as expected, and also we can see that the resonant frequency is almost the same in both situations, showing that the Δ factor is relevant mainly in the quasi-static limit.

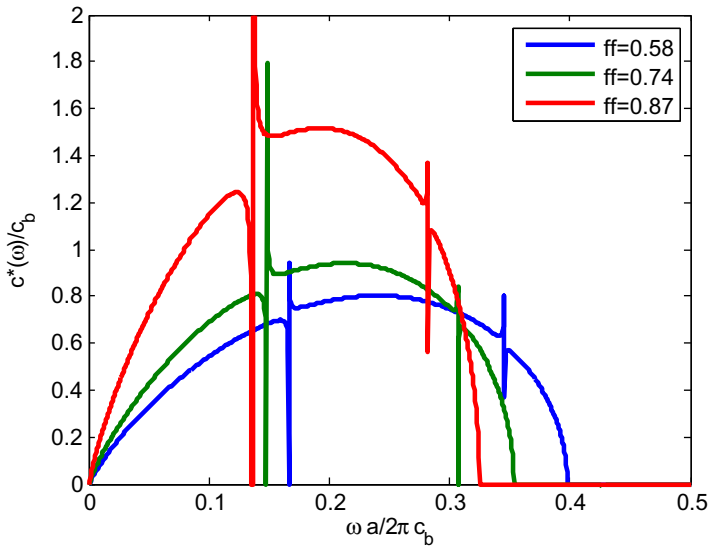

Figure 2. Imaginary part of the effective sound speed for a medium consisting of a hexagonal lattice of air cylinders in a water background. The lattice constant is a.

Finally, figure 2 shows the imaginary part of the effective speed of sound. As the effective bulk modulus is negative for the whole range of frequencies considered as the homogenization limit, the effective speed of sound is always purely imaginary. It becomes real only in the narrow region where the effective mass density is also negative, due to the local resonance. This sharp resonance can be observed numerically; however, it is hard to believe that this could be observed experimentally. Thus, we can conclude that the system of air cylinders in a water background will always be a non-propagating medium in the low-frequency limit.

3.2. Anisotropic metamaterials

Expressions obtained in the last section are not valid in the case of anisotropic lattices (i.e. in lattices other than the hexagonal or the square). Expressions for the anisotropic mass density were reported in the quasi-static limit and they depend on the cylinder's parameters and the lattice geometry [38]. It can be shown that even neglecting the terms of multiple scattering interaction, mass anisotropy appears for non-symmetric lattices. The components of the effective mass density tensor are

$$\rho_{xx}^{*-1}(\omega) = \frac{1 - f^2\eta^2(\omega)(A+1)^2}{1 + 2f\eta(\omega) + f^2\eta^2(\omega)(1-A^2)}\rho_b^{-1}, \tag{18a}$$

$$\rho_{yy}^{*-1}(\omega) = \frac{1 - f^2\eta^2(\omega)(A-1)^2}{1 + 2f\eta(\omega) + f^2\eta^2(\omega)(1-A^2)}\rho_b^{-1}, \tag{18b}$$

where A is the anisotropy factor introduced in [38] and $\eta(\omega)$ is given by equation (14) with $\rho_a = \rho_a(\omega)$. It is assumed that the coordinate axes are oriented along the principal axes of the tensor ρ_{ik}.

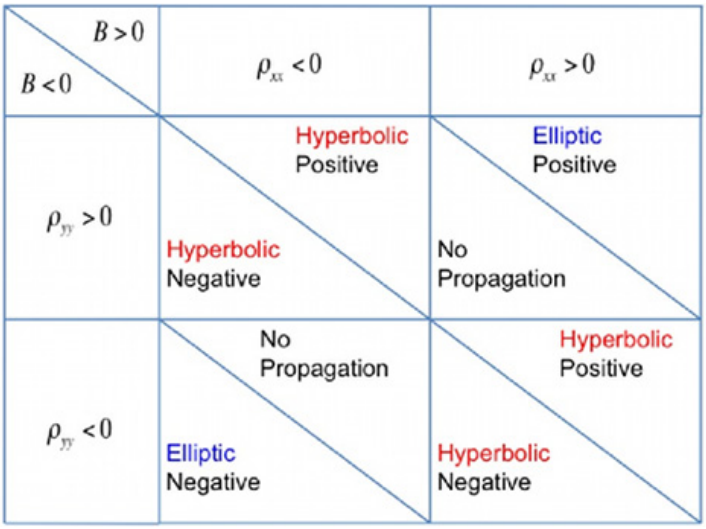

Figure 3. Summary of the different types of propagation inside acoustic metamaterials.

The expression for the effective bulk modulus remains the same as that in the previous section, so that we can obtain the tensor for the effective speed of sound [38] as follows:

$$\frac{c_{ij}^{*2}}{c_b} = \rho_{ij}^{*-1} B^*. \tag{19}$$

Note that the anisotropic mass density tensor can have both the principal values of the same sign (negative or positive) or they can be of opposite signs.

Therefore, for the acoustic refractive index, we have

$$n^*(\theta) = \frac{1}{\pm\sqrt{c^{*2}(\theta)}} = \frac{1}{\pm\sqrt{c_{xx}^{*2}\cos^2\theta + c_{yy}^{*2}\sin^2\theta}}, \tag{20}$$

where θ defines the direction of propagation of acoustic waves in the effective medium. The refractive index surface $n^*(\theta)$ can be either elliptical, hyperbolic or imaginary, and also positive or negative, depending on the sign of B^* and the components of the mass density tensor.

When both the diagonal components of the mass density tensor have the same sign, but have signs different from that of the effective bulk modulus, the refractive index becomes imaginary and there is no sound propagation. When the signs are the same as that of the effective bulk modulus, the refractive index becomes elliptical—or circular in the case of isotropic media—and we have normal refraction or negative refraction, depending on the sign of the components of the mass density tensor.

If the components of the mass density tensor are of different signs, the refractive index surface is hyperbolic, and the sign of the square root in equation (20) is the same as that of B^*. The propagation of waves in this medium will be determined by the component of the mass density tensor that has the same sign as B^*. In this case the refractive index surface is hyperbolic, positive or negative.

Figure 3 summarizes all types of propagation regimes allowed in metamaterials. Note that, for a given frequency, it is not possible to have a positive index in one direction and a negative

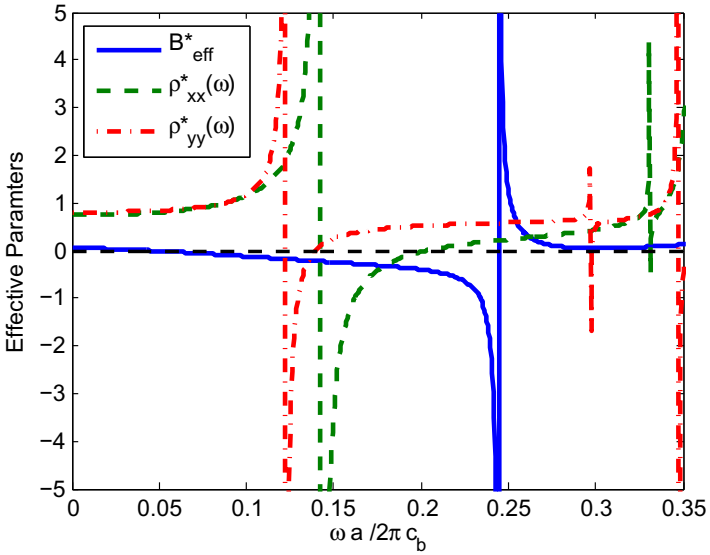

Figure 4. Effective parameters, normalized to those of the background, of fluid-like cylinders distributed in a rectangular lattice with $b = 2a$. The parameters of the cylinders are $\rho_a = 0.5\rho_b$, $B_a = 0.02B_b$ and $R_a = 0.49a$. Note that the two narrow multipolar resonances observed at about $\omega a/2\pi c_b = 0.3$ and 0.35 are located in a frequency region where the homogenization hypothesis is not valid. The thin horizontal line is a guide to the eyes defining the zero of the vertical axis.

index in another direction, since the character of the propagation is determined by the bulk modulus, whose sign is determined by the operating frequency.

The mass density tensor and the scalar bulk modulus are plotted in figure 4 for a system of cylinders with $B_a = 0.02B_b$ and $\rho_a = 0.5\rho_b$. The underlying lattice is rectangular with $b = 2a$ and its filling fraction $f = 0.3771$, corresponding to cylinders with radius $R_a = 0.49a$. Figure 5 depicts the real part of the corresponding components of the sound speed tensor. We observe that from $\omega a/2\pi c_b$ =0 to 0.05, the refractive index is elliptical and positive; then a region of non-propagation appears, where the bulk modulus is negative and the two components of the mass density tensor are positive, leading to a refractive index imaginary for all directions. Finally, two frequency regions with a negative hyperbolic index appear since the mass density tensors have two resonances and still a negative effective bulk modulus.

Multiple scattering interactions have been included within this analysis; however, their effects are negligible at low frequencies. Note also that as $\rho_a = 0.5\rho_b$ we have that $\eta = -1/3$, which is three times smaller than the air–water case, where $\eta \approx -1$, which makes multiple scattering interactions irrelevant in general.

This simple example shows the variety and complexity of the propagation characteristics of anisotropic metamaterials. It is obvious that correct design of both elliptic and hyperbolic refractive indices should be done by properly engineering the constituent scatterers as well as the chosen underlying lattice.

4. Application to electromagnetic metamaterials

The vectorial nature of EM waves makes the problem more complex, but in two dimensions (2D) the EM field can be decomposed into the TE and TM modes, leading to the same wave equation

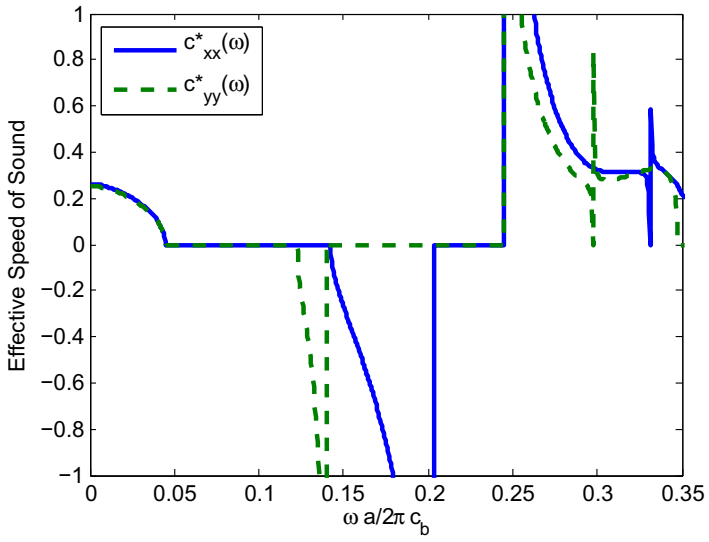

Figure 5. Real part of the effective speed of the sound tensor of the medium described in figure 4 as a function of frequency. Note that we can have both components positive, or one negative and the other imaginary (the real part is equal to zero in this plot). It is impossible to have one component negative and the other positive (see text). The horizontal dashed line is a guide to the eyes.

as that for scalar acoustic waves. Now P in equations (1) and (5) is the z component of the electric (magnetic) field for the TE (TM) mode, and $(\rho, B) = (\mu, \varepsilon^{-1})$ for the TE mode and $(\rho, B) = (\varepsilon, \mu^{-1})$ for the TM mode.

Although both problems are mathematically equivalent, physically they are quite different. The numerical values and ranges of the material parameters ρ, B and μ, ε are not the same in both fields; therefore it is worth studying them separately.

For EM structures in the dilute regime (low filling fractions), we can assume that $\Delta \approx 1$ and the effective parameters for the TE mode are

$$\frac{\varepsilon_b}{\varepsilon_a^{\mathrm{TE}}(\omega)} = \frac{k_b^2 R_a^2}{2} \ln k_b R_a + \frac{k_a R_a}{2} \frac{J_0(k_a R_a)}{J_1(k_a R_a)} \frac{\varepsilon_b}{\varepsilon_a}, \tag{21a}$$

$$\frac{\mu_a^{\mathrm{TE}}(\omega)}{\mu_b} = \frac{1}{k_a R_a} \frac{J_1(k_a R_a)}{J_1'(k_a R_a)} \frac{\mu_a}{\mu_b}. \tag{21b}$$

For the TM mode,

$$\frac{\mu_b}{\mu_a^{\mathrm{TM}}(\omega)} = \frac{k_b^2 R_a^2}{2} \ln k_b R_a + \frac{k_a R_a}{2} \frac{J_0(k_a R_a)}{J_1(k_a R_a)} \frac{\mu_b}{\mu_a}, \tag{22a}$$

$$\frac{\varepsilon_a^{\mathrm{TM}}(\omega)}{\varepsilon_b} = \frac{1}{k_a R_a} \frac{J_1(k_a R_a)}{J_1'(k_a R_a)} \frac{\varepsilon_a}{\varepsilon_b}. \tag{22b}$$

These expressions show that even when the cylinders are non-magnetic ($\mu_a = \mu_b = \mu_0$), we can have a magnetic response within a given frequency range. This is a well-known phenomenon called mesomagnetism [42–44].

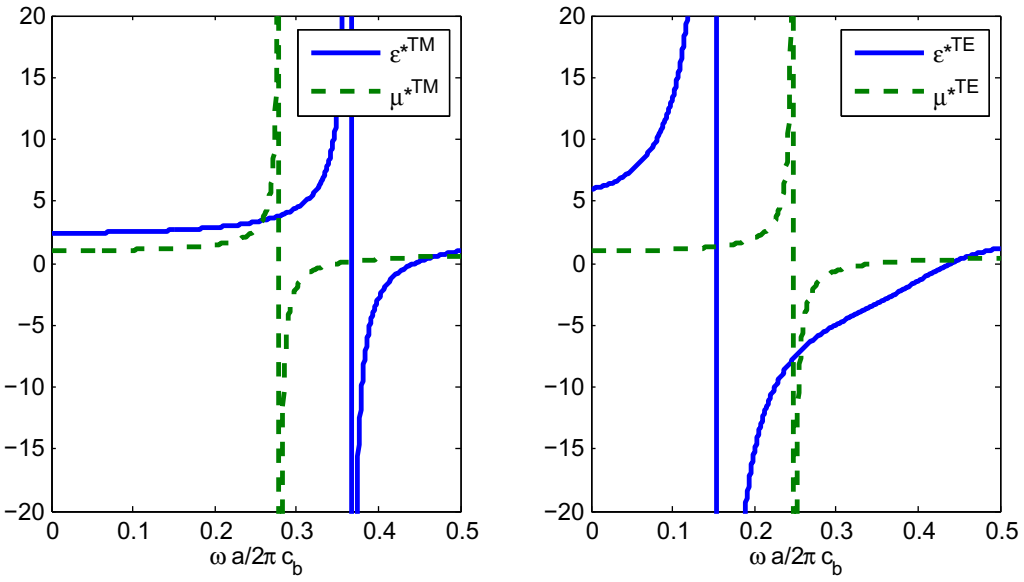

Figure 6. Effective constitutive parameters of a square lattice of dielectric cylinders with radius $R_a = 0.4a$ and $\varepsilon_a = 11\varepsilon_b$. The resonances of the effective permeability and permittivity for the TM case are so sharp that they do not allow the system to present negative refraction for that polarization. However, the TE polarization is allowed within a wide range of frequencies.

Also these equations show that, as a function of frequency, the same cylinders have different responses for the TE and the TM modes, exhibiting different constitutive parameters that are equal only when $\omega \to 0$, i.e.

$$\lim_{\omega\to 0} \varepsilon_a^{\mathrm{TE}}(\omega) = \varepsilon_a^{\mathrm{TM}}(\omega) = \varepsilon_a, \tag{23}$$

$$\lim_{\omega\to 0} \mu_a^{\mathrm{TE}}(\omega) = \mu_a^{\mathrm{TM}}(\omega) = \mu_a. \tag{24}$$

The effective medium made of a cluster of these scatterers will present different constitutive parameters for each of the polarizations, so that, applying the results of section 3, we obtain

$$\varepsilon^{*\mathrm{TE}}(\omega) = (1-f)\varepsilon_b + f\varepsilon_a^{\mathrm{TE}}, \tag{25a}$$

$$\mu^{*\mathrm{TE}}(\omega) = \frac{\mu_a^{\mathrm{TE}}(\omega)(1+f) + \mu_b(1-f)}{\mu_a^{\mathrm{TE}}(\omega)(1-f) + \mu_b(1+f)}\mu_b, \tag{25b}$$

$$\mu^{*\mathrm{TM}}(\omega) = (1-f)\mu_b + f\mu_a^{\mathrm{TM}}, \tag{25c}$$

$$\varepsilon^{*\mathrm{TM}}(\omega) = \frac{\varepsilon_a^{\mathrm{TM}}(\omega)(1+f) + \varepsilon_b(1-f)}{\varepsilon_a^{\mathrm{TM}}(\omega)(1-f) + \varepsilon_b(1+f)}\varepsilon_b. \tag{25d}$$

Figure 6 depicts the effective constitutive parameters for a square lattice of dielectric cylinders with $\varepsilon_a = 11\varepsilon_b$ and $R_a = 0.4a$. Note that although $\mu_a = \mu_b = \mu_0$ there is a strong magnetic resonance for both polarizations. However, we note that the resonance of $\varepsilon^{\mathrm{TM}}$, at

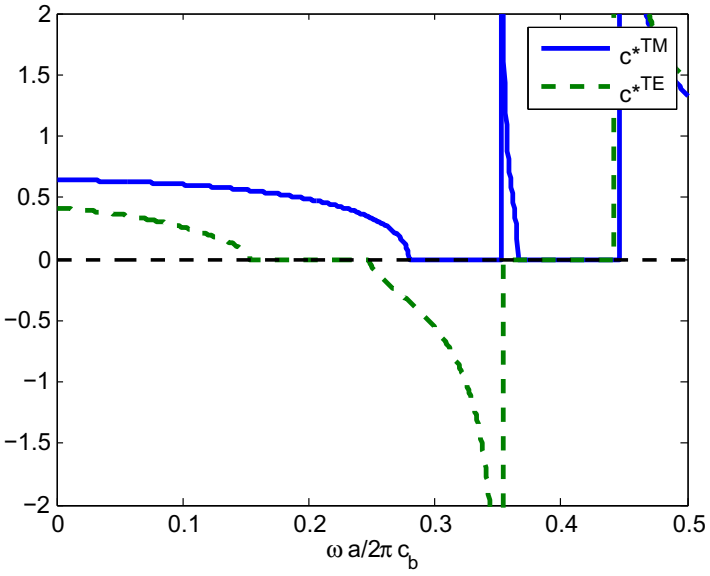

Figure 7. Effective speed of light normalized to that of the background for both the TE and TM modes. As we can see, there is no negative refraction for the TM mode (see text). The regions where there is no solution correspond to those where ε and μ have different signs, so that the speed of sound is purely imaginary.

$\lambda \lesssim 2.6a$, is beyond the homogenization condition ($\lambda \geqslant 4a$) [36]. Probably this resonance could not be observed.

Figure 7 shows the effective speed of light (relative to that of the background) for this system. Note that only the TE polarization presents negative speed of light (or negative refraction index). This phenomenon is due to the fact that the resonance of $\varepsilon^{\mathrm{TM}}$ is too far and too sharp to overlap with that of μ^{TM}. If we would like to have negative refraction in both polarizations, we should employ anisotropic cylinders, as we did for the acoustic case.

If the cylinder's permittivity is given by a tensor of the form

$$\hat{\varepsilon}_a = (\varepsilon_{ar}, \varepsilon_{a\theta}, \varepsilon_{az}), \tag{26}$$

the expressions for the frequency-dependent constitutive parameters are now

$$\frac{\varepsilon_b}{\varepsilon_a^{\mathrm{TE}}(\omega)} = \frac{k_b^2 R_a^2}{2} \ln k_b R_a + \frac{k_a^{\mathrm{TE}} R_a}{2} \frac{J_0(k_a^{\mathrm{TE}} R_a)}{J_1(k_a^{\mathrm{TE}} R_a)} \frac{\varepsilon_b}{\varepsilon_{az}}, \tag{27a}$$

$$\frac{\mu_a^{\mathrm{TE}}(\omega)}{\mu_b} = \frac{1}{k_a^{\mathrm{TE}} R_a} \frac{J_1(k_a^{\mathrm{TE}} R_a)}{J_1'(k_a^{\mathrm{TE}} R_a)} \frac{\mu_a}{\mu_b}, \tag{27b}$$

$$\frac{\mu_b}{\mu_a^{\mathrm{TM}}(\omega)} = \frac{k_b^2 R_a^2}{2} \ln k_b R_a + \frac{k_a^{\mathrm{TM}} R_a}{2} \frac{J_0(k_a^{\mathrm{TM}} R_a)}{J_1(k_a^{\mathrm{TM}} R_a)} \frac{\mu_b}{\mu_a} \tag{27c}$$

$$\frac{\varepsilon_a^{\mathrm{TM}}(\omega)}{\varepsilon_b} = \frac{1}{k_a^{\mathrm{TM}} R_a} \frac{J_\gamma(k_a^{\mathrm{TM}} R_a)}{J_\gamma'(k_a^{\mathrm{TM}} R_a)} \frac{\varepsilon_{a\theta}}{\varepsilon_b}, \tag{27d}$$

where $k_a^{\mathrm{TE}} = \omega\sqrt{\varepsilon_{za}\mu_a}$, $k_a^{\mathrm{TM}} = \omega\sqrt{\varepsilon_{a\theta}\mu_a}$ and $\gamma^2 = \varepsilon_{a\theta}/\varepsilon_{ar}$.

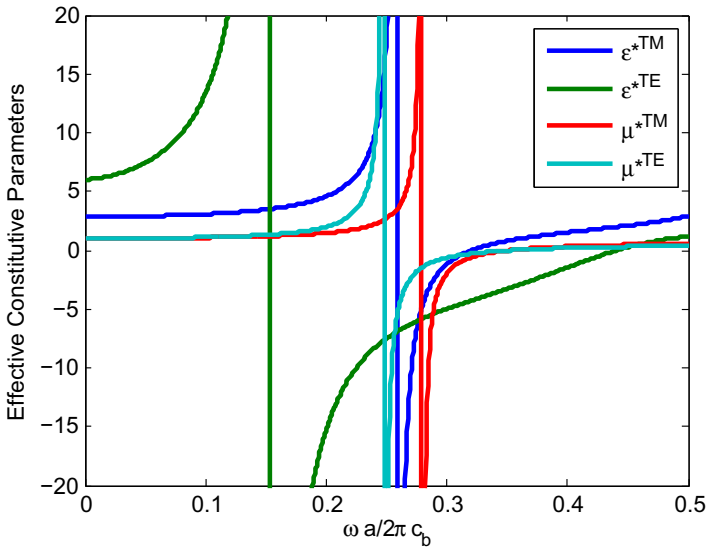

Figure 8. Frequency shift to the left of the $\varepsilon^{\mathrm{TM}}$ resonance due to anisotropy of the cylinder. As we see, there is a frequency region in which all the constitutive parameters for the two modes (TE and TM) are negative, so that we have a region of total negative refraction.

These expressions allow us to shift the resonance of $\varepsilon^{\mathrm{TM}}$ to lower values just by increasing $\varepsilon_{\mathrm{ar}}$ and keeping the rest of the system unaltered, in the same way as we did for the acoustic case. Note that due to the correspondence $\rho_r \to \varepsilon_\theta^{\mathrm{TM}}$ and $\rho_\theta \to \varepsilon_r^{\mathrm{TM}}$, we need to increase the value of ε_{ar} in the EM case. Thus, as we increase it, the anisotropy factor γ goes to zero, and the resonance moves to the left.

Figure 8 shows the same system as that in figure 6 but with anisotropic cylinders, where $\varepsilon_r = 200\varepsilon_\theta$ and $\varepsilon_\theta = \varepsilon_z = 11\varepsilon_b$. A periodic array of parallel carbon nanotubes embedded in a background material with isotropic permittivity ϵ_b is an example of this type of system [45]; the cylinders are rolled up from an anisotropic dielectric sheet characterized by a tensor that in dielectric coordinates is represented by a diagonal matrix with elements $\varepsilon_{a\theta} = \varepsilon_{az}$ and $\varepsilon_{\mathrm{ar}} = \varepsilon_b$. Note how all the resonances keep their positions but ϵ^{TM}, which now moves to the left reaching the μ^{TM}-resonance, leading, therefore, to an effective medium with negative refraction. The effective speed of light is depicted in figure 9, where it is obvious now that both polarizations present negative refraction properties within the same frequency range.

5. Summary

In summary, we present multiple scattering formulation of acoustic metamaterials. This formulation is based on a homogenization theory in the low-frequency limit, in which we allow the wavenumber in the background to be arbitrarily small while the wavenumber inside the scatterers remains finite.

In general, it is shown that ordered or disordered arrays of sound scatterers can behave, in the low-frequency limit, like effective fluid-like materials with either positive or negative acoustic parameters, where these parameters are the scalar bulk modulus and the tensorial mass

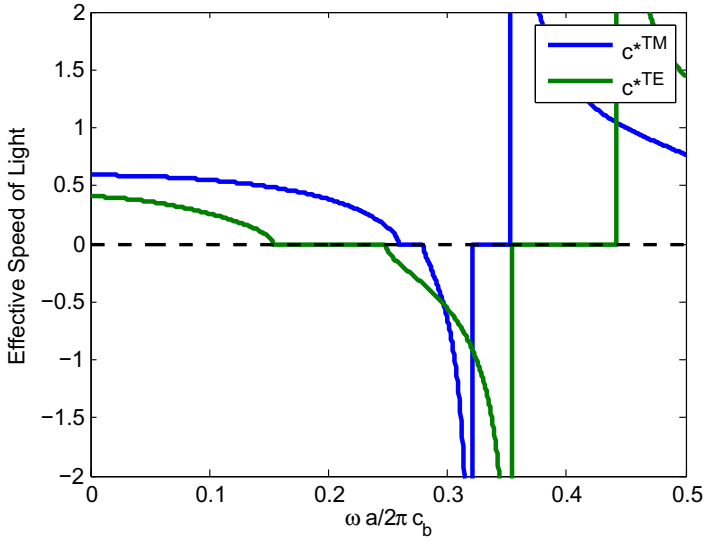

Figure 9. Effective speed of light for both TE and TM modes for the system of figure 8. It is clear that there is a region of total negative refraction, thanks to the frequency shift of the $\varepsilon^{\mathrm{TM}}$ resonance caused by anisotropy (see text).

density. The behavior of the effective medium depends, among other factors, on the surface fields at the scatterer. Therefore, it is possible to improve or manage the frequency response of the effective medium with complex scatterers, like fluid-like shells or anisotropic fluid-like materials.

Examples of these scatterers have been analyzed, showing that they present negative effective parameters whenever the theory predicts them, verifying therefore the formulation presented. Also, it has been shown how these complex scatterers can be used to tune the effective parameters of the medium.

The homogenization theory developed for acoustic waves has been extended to EM waves in 2D. It was shown that an equivalent type of scatterers can also be used in dielectric materials to tailor the effective medium response.

In conclusion, the theory presented not only explains the metamaterial behavior found so far in the literature, but also gives the basis for improving this behavior with more complex scatterers.

Acknowledgments

This work was partially supported by the US Office of Naval Research under grant number N000140910554 and the Spanish Ministry of Science and Innovation under contract numbers TEC2010-19751 and CSD2008-66 (the CONSOLIDER program). Daniel Torrent also acknowledges support from the contract provided by the program 'Campus de Excelencia Internacional' 2010 UPV.

Appendix A. Scatterers with local negative parameters

This appendix presents the application of formulae developed in section 2.1 to three different types of scatterers whose metamaterial behavior has been reported so far. The first one

corresponds to a homogeneous fluid cylinder such that $c_a \ll c_b$, the condition that grants $k_b \ll k_a$. The second is also a homogeneous fluid cylinder but with cylindrical anisotropy. These types of cylinders have already been studied for cloaking devices, radial wave crystals [46], hyperlenses [16] and low-frequency resonators [47]. They are employed here as examples to see how they can be used to tune the resonance of the dynamical mass density of a metamaterial. Finally, the third example shows that fluid-like shells can work as Helmholtz resonators, obtaining from them negative bulk modulus, but also they can work as metamaterials with negative mass density.

In order to improve the metamaterial frequency response, complex scatterers should be employed but a full analysis of this type is beyond the scope of the present work.

A.1. Homogeneous and isotropic scatterers

For a homogeneous scatterer with parameters ρ_a and B_a the field inside the scatterer is given in terms of the Bessel functions. Therefore, after some algebra, the frequency-dependent parameters are

$$B_a(\omega)/B_b = \frac{k_b^2 R_a^2}{2} \ln k_b R_a + \frac{k_a R_a}{2} \frac{J_0(k_a R_a)}{J_1(k_a R_a)} \frac{B_a}{B_b}, \tag{A.1a}$$

$$\rho_a(\omega)/\rho_b = \frac{1}{k_a R_a} \frac{J_1(k_a R_a)}{J_1'(k_a R_a)} \frac{\rho_a}{\rho_b}, \tag{A.1b}$$

where $k_a = \omega\sqrt{\rho_a/B_a}$. Note that for $k_a \to 0$ we recover the static cylinder's parameters.

Metamaterial behavior appears when $k_b R_a \ll 1$, while $k_a R_a$ is not necessarily small. This condition occurs when $c_a \ll c_b$, i.e. when the wavelength in the background is several times larger than that inside the scatterer.

Figure A.1 plots the frequency-dependent parameters described by equations (A.1*a*) and (A.1*b*) for a soft scatterer with $B_a = 0.005 B_b$ and $\rho_a = 0.5\rho_b$. These values give $c_a = 0.1 c_b$ for the speed of sound of the scatterer. This relation locates the resonances in the low-frequency limit, as can be seen in the figure.

From (A.1*b*) we obtain that the region of negativity for $\rho_a(\omega)$ is determined by the first zeros of $J_1(k_a R_a)$ and $J_1'(k_a R_a)$, which are $\alpha = 3.8317$ and $\alpha' = 1.8412$, respectively [40]. Then, this region is

$$\frac{1.8412 c_a}{R_a} < \omega_- < \frac{3.8317 c_a}{R_a}, \qquad \Delta\omega_- \approx \frac{2 c_a}{R_a}. \tag{A.2}$$

Therefore, if we want to locate the frequency region in the low-frequency limit, we have to decrease c_a (for fixed R_a). But, as a consequence, the bandwidth will decrease because the resonance becomes sharper.

These types of scatterers are possible only in an acoustically more dense background, like water, where we can get such a low bulk modulus and density. If we need to get metamaterials in an air or gas background another approach should be used instead.

A.2. Homogeneous and anisotropic scatterers

Sometimes it is not possible to obtain materials with sound speed smaller than a certain value. If we want to decrease the frequency at which the mass density becomes negative, fluid-like

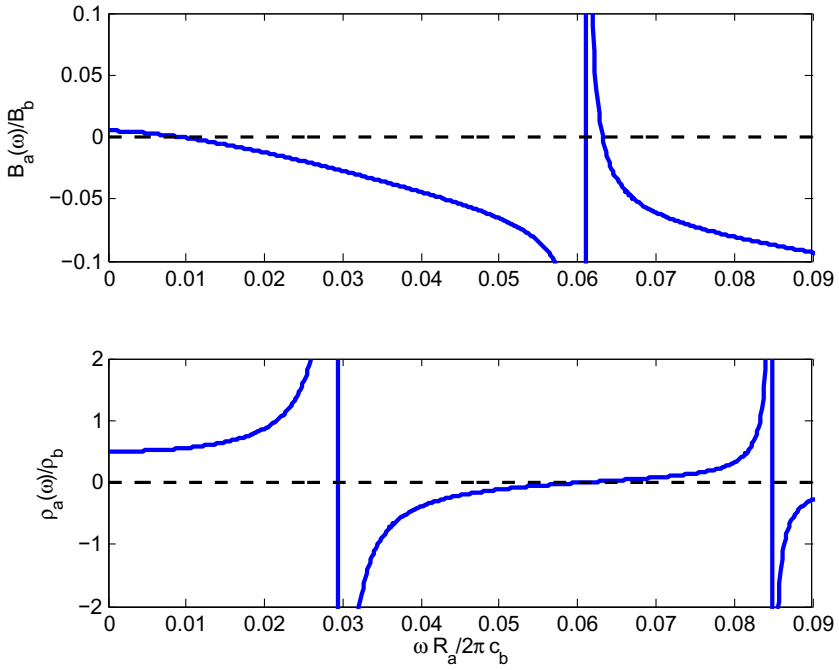

Figure A.1. Frequency-dependent parameters of a homogeneous and isotropic fluid-like cylinder with $B_a = 0.005B_b$ and $\rho_a = 0.5\rho_b$. A low-frequency resonance is observed for both parameters, leading to negative refractive index behavior.

cylinders with circular anisotropy can be used in order to shift the resonance to lower frequencies [48].

Anisotropic cylinders are characterized by a scalar bulk modulus B_a and a tensorial mass density whose components are constant when referred to a cylindrical coordinate system, $\hat{\rho}_a = (\rho_r, \rho_\theta)$. In these cylinders the pressure field is described in terms of the Bessel functions of real order γq,

$$\psi_q(r, \omega) = J_{\gamma q}(k_a r), \tag{A.3}$$

where $\gamma = \sqrt{\rho_r/\rho_\theta}$ is the anisotropy factor.

Since this type of anisotropy does not break azimuthal symmetry, the method developed here remains valid. Thus, when $q = 0$ the field distribution is the same as that of an isotropic cylinder (because $J_{\gamma q}$ for $q = 0$ is J_0), the frequency-dependent bulk modulus is also given by equation (A.1*a*). However, (A.1*b*) now becomes

$$\rho_a(\omega)/\rho_b = \frac{1}{k_a R_a} \frac{J_\gamma(k_a R_a)}{J'_\gamma(k_a R_a)} \frac{\rho_a}{\rho_b} \tag{A.4}$$

and, as we let the anisotropy factor γ be smaller than one, the dipolar resonance $q = 1$ becomes closer to the monopolar one,

$$\lim_{\gamma \to 0} J_\gamma(k_a r) \approx J_0(k_a r), \tag{A.5}$$

and the resonant frequency decreases.

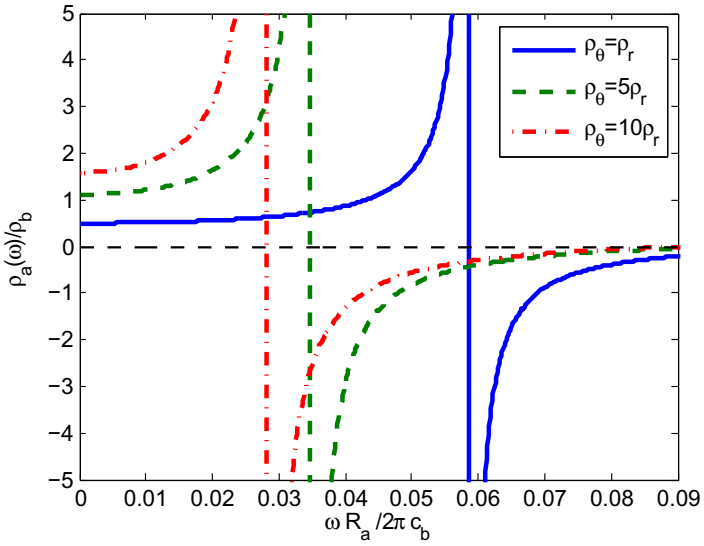

Figure A.2. Effective dynamical mass density of an anisotropic fluid-like cylinder for three different anisotropy ratios. The radial component of the sound speed tensor is $c_r = 0.2c_b$ in the three examples. Note that the growth of the anisotropy ratio leads to a lower resonant frequency.

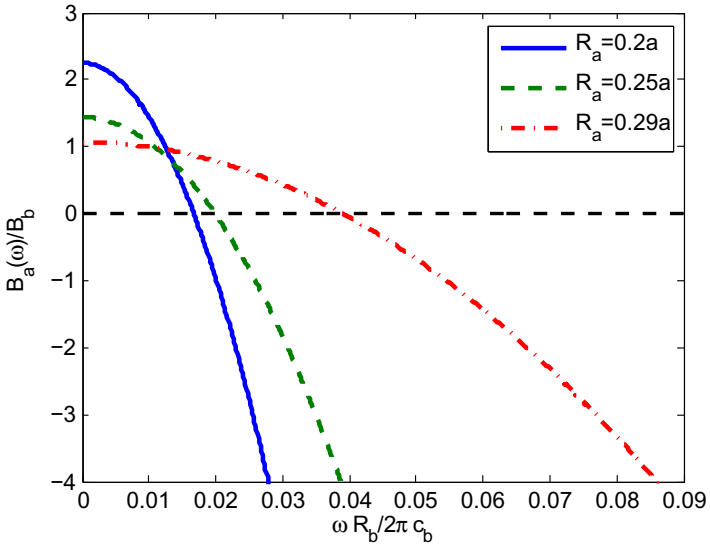

Figure A.3. Effective bulk modulus of a water shell scatterer embedded in air. The outer radius of the shell is $R_b = 0.3a$. Effective values are obtained for three different inner radii R_a.

This effect is clearly observed in figure A.2, where the frequency-dependent mass density is plotted for three different ρ_r/ρ_θ ratios. Note how the resonance of the density moves to lower frequencies as we increase the value of ρ_θ (so that we decrease the anisotropy factor γ).

These types of strongly anisotropic fluid-like cylinders have already been used by Li *et al* [16] to build an acoustic hyperlens and have been recently characterized for different anisotropy ratios in [47], showing also the same frequency shift.

A.3. Fluid-like shells as Helmholtz resonators

Let us assume now that we have a fluid-like cylinder of radius R_a and parameters ρ_a and B_a. If this cylinder is enclosed by another of radius $R_b > R_a$ and parameters ρ_s and B_s, we have a fluid-like shell. Obviously this is an idealization, because such a structure cannot be realized with common fluids. However, on the one hand, if the shell is an elastic material, this can sometimes be a good approximation; on the other hand, if the fluids are 'metafluids' [49–51], the structure can be easily fabricated.

These structures behave like Helmholz resonators [24, 26]. Here we give a more rigorous derivation of the resonance frequency.

After applying the correct boundary conditions, the impedance factor χ_q of a fluid-like shell is given by

$$\chi_q = \frac{\rho_s c_s}{\rho_b c_b} \frac{J_q(k_s R_b) + T_q^a Y_q(k_s R_b)}{J_q'(k_s R_b) + T_q^a Y_q'(k_s R_b)}, \tag{A.6}$$

where

$$T_q^a = -\frac{\chi_q^a J_q'(k_s R_a) - J_q(k_s R_a)}{\chi_q^a H_q'(k_s R_a) - H_q(k_s R_a)} \tag{A.7}$$

and

$$\chi_q^a = \frac{\rho_a c_a}{\rho_s c_s} \frac{J_q(k_a R_a)}{J_q'(k_a R_a)}. \tag{A.8}$$

The parameters of the shell are ρ_s and c_s, while those of the enclosed cylinder are ρ_a and c_a.

For $q = 0$ and $k_s \to 0$, the inner T matrix T_0^a is equal to

$$T_0^a \approx \frac{\pi R_a^2 k_s^2}{4} \frac{\left[1 - \frac{B_s}{B_a}\right]}{\xi_a}, \tag{A.9}$$

where

$$\xi_a = 1 + \frac{B_s}{B_a} \frac{k_s^2 R_a^2}{2} \ln k_s R_a. \tag{A.10}$$

Thus the impedance factor of the shell can be approximated by

$$\chi_0 \approx -\frac{2}{k_b R_b} \frac{B_s}{B_b} \frac{1 + \frac{k_s^2 R_a^2}{2}\left[1 - \frac{B_s}{B_a}\right] \ln k_s R_b / \xi_a}{1 - \frac{R_a^2}{R_b^2}\left[1 - \frac{B_s}{B_a}\right] / \xi_a}, \tag{A.11}$$

which can be zero only for $B_s/B_a \gg 1$ and consequently

$$\xi_a \approx \frac{k_s^2 R_a^2}{2} \frac{B_s}{B_a} \ln k_s R_b, \tag{A.12}$$

which defines a cut-off frequency ω_c:

$$\omega_c = \frac{c_a}{R_a} \sqrt{\frac{2\rho_a}{\rho_s \ln(R_b/R_a)}}. \tag{A.13}$$

If the shell is soft, i.e. if $B_s/B_a \ll 1$, a negative bulk modulus appears as in the case of a homogeneous cylinder, and the shell nature of the scatterer is not relevant. In that case, as $R_b \to R_a$ the impedance factor is reduced to

$$\chi_0 \approx -\frac{2}{k_b R_b}\frac{B_s}{B_b}\frac{1}{1-\frac{R_a^2}{R_b^2}\left[1-\frac{B_s}{B_a}\right]} \approx -\frac{2}{k_b R_b}\frac{B_a}{B_b}, \tag{A.14}$$

and the bulk modulus cannot be negative. However, we will see now that in that case the density can be negative.

When $q = 1$ the inner T matrix T_1^a is approximated by

$$T_1^a \approx -\frac{\pi R_a^2 k_s^2}{4}\frac{\rho_a - \rho_s}{\rho_a + \rho_s}. \tag{A.15}$$

The density becomes negative once the denominator of χ_1 vanishes, i.e. when

$$J_1'(k_s R_b) + T_1^a Y_1'(k_s R_b) \approx \frac{1}{2}\left[1 - \frac{k_s^2 R_b^2}{4} - \frac{R_a^2}{R_b^2}\frac{\rho_a - \rho_s}{\rho_a + \rho_s}\right] = 0. \tag{A.16}$$

This expression gives the cut-off frequency for the negative density

$$\omega_c^2 = \frac{4c_s^2}{R_b^2}\left[1 - \frac{R_a^2}{R_b^2}\frac{\rho_a - \rho_s}{\rho_a + \rho_s}\right], \tag{A.17}$$

where we now need $\rho_s \ll \rho_a$.

Appendix B. Multiple scattering and the Δ factor

This subsection briefly explains how the multiple scattering contribution appears in the effective parameters by means of the so-called Δ factor. First, we describe the multiple scattering formulation of the band structure calculation for a 2D lattice of identical cylinders. Afterwards, we analyze the low-frequency limit of the band structure in order to obtain the effective speed of sound of the homogenized medium. Finally, we derive the effective mass density from the effective speed of sound obtained previously.

Given a cluster of N cylinders located at arbitrary positions in 2D, multiple scattering theory assumes that the total scattered field is a superposition of the scattered fields by all the cylinders in the cluster

$$P^{sc} = \sum_{\alpha=1}^{N} P_\alpha^{sc}. \tag{B.1}$$

The scattered field P_α^{sc} is the response of the cylinder α to a given incident field, which in this case is the field scattered by the rest of the cylinders—no external field is considered here since we are looking for the eigenmodes of the system. The response of one cylinder to the incident field is defined, as explained in the text, by the T matrix. Thus, we have

$$P_\alpha^{sc} = \boldsymbol{T}_\alpha P_\alpha^0 = \boldsymbol{T}_\alpha \sum_{\beta\neq\alpha} \boldsymbol{G}_{\alpha\beta} P_\beta^{sc}, \tag{B.2}$$

where $\boldsymbol{T}_\alpha = [T_q]_\alpha$ is the T matrix of the α cylinder (assumed here to be a diagonal matrix) and $\boldsymbol{G}_{\alpha\beta} = [G_{qs}]_{\alpha\beta}$ are the coefficients that translate the scattered wave functions from the β reference frame to the α one. If all the cylinders are identical and arranged in a regular lattice,

such that $\boldsymbol{R}_\alpha = \alpha_1 \boldsymbol{a}_1 + \alpha_2 \boldsymbol{a}_2$, with α_1, α_2 being integers, and we let the number of cylinders N be infinite, Bloch's theorem relates the field scattered by a cylinder α to the scattered field by another cylinder β by means of the Bloch wave vector $\boldsymbol{K}$:

$$P_\beta^{\mathrm{sc}} = \mathrm{e}^{\mathrm{i}\boldsymbol{K}\cdot\boldsymbol{R}_{\alpha\beta}} P_\alpha^{\mathrm{sc}}. \tag{B.3}$$

Thus, equation (B.2) now becomes

$$P_\alpha^{\mathrm{sc}} = \boldsymbol{T}_\alpha \sum_{\beta\neq\alpha} \boldsymbol{G}_{\alpha\beta}\, \mathrm{e}^{\mathrm{i}\boldsymbol{K}\cdot\boldsymbol{R}_{\alpha\beta}} P_\alpha^{\mathrm{sc}}, \tag{B.4}$$

which is equivalent to

$$(\boldsymbol{I} - \boldsymbol{T}_\alpha \boldsymbol{S}_\alpha) P_\alpha^{\mathrm{sc}} = 0, \tag{B.5}$$

where $\boldsymbol{S}_\alpha(\omega, \boldsymbol{K}) = \sum_{\beta\neq\alpha} \boldsymbol{G}_{\alpha\beta}\, \mathrm{e}^{\mathrm{i}\boldsymbol{K}\cdot\boldsymbol{R}_{\alpha\beta}}$. The above system of equations has nontrivial solutions as long as

$$|\boldsymbol{I} - \boldsymbol{T}\boldsymbol{S}| = |\delta_{qs} - T_q S_{qs}| = 0, \tag{B.6}$$

whose solutions define the band structure of the periodic arrangement, $\boldsymbol{K} = \boldsymbol{K}(\omega)$. As can be seen, this band structure or dispersion relation depends on the structure of the lattice through the lattice sums S_{qs} and on the nature of the cylinders through the T matrix. It is well known that in the low-frequency limit this dispersion relation becomes linear, defining the slope of this line the effective speed of sound c^* as

$$\lim_{\omega\to 0} \frac{\boldsymbol{K}(\omega)}{\omega} = \lim_{k_b\to 0} \frac{\boldsymbol{K}}{k_b c_b}, \tag{B.7}$$

where $k_b = \omega/c_b$ is the background's wavenumber and $\boldsymbol{u}$ is a unit vector in the direction of the wavevector $\boldsymbol{K}$. The effective speed of sound $c^*(\boldsymbol{u})$ depends on the direction of propagation and, therefore, the effective medium is anisotropic.

A semi-analytical expression for the effective speed of sound c^* can be found by analyzing the low-frequency limit of equation (B.6),

$$\lim_{\omega\to 0} |\boldsymbol{I} - \boldsymbol{T}\boldsymbol{S}| = |\delta_{qs} - \hat{T}_q \hat{S}_{qs}| = 0, \tag{B.8}$$

where neither $\hat{T}_q$ nor $\hat{S}_{qs}$, given by

$$\hat{T}_q = \lim_{k_b\to 0} \frac{T_q}{k_b^{2|q|}}, \tag{B.9}$$

$$\hat{S}_{qs} = \lim_{k_b\to 0} S_{qs} k_b^{|q|+|s|} \tag{B.10}$$

is a function of ω, as we have taken the long-wavelength limit ($\omega \to 0$) and only those terms different from zero are kept. The expressions for these asymptotic forms can be found in [38].

The secular equation (B.8) is, in principle, of infinite order since the multipolar terms q, s run from $-\infty$ to ∞. Even truncating these indices to $\pm Q_{\max}$ the determinant is too complex to be solved analytically. However, as shown in [38], only the terms in $\hat{S}_{qs}$ such that $q, s = 0, \pm 1$ contain information on the effective speed of sound c^*, which is the only unknown in that equation; thus, the matrix $M_{qs} = \delta_{qs} - \hat{T}_q \hat{S}_{qs}$ can be factorized into four blocks such that

$$M = \begin{pmatrix} \boldsymbol{A}_{3\times 3} & \boldsymbol{B}_{3\times Q} \\ \boldsymbol{C}_{Q\times 3} & \boldsymbol{D}_{Q\times Q} \end{pmatrix}, \tag{B.11}$$

where the subindex of each matrix indicates its dimensions and only matrix $\boldsymbol{A}$ contains the variable c^*. It can be seen that the condition $\det M = 0$ is equivalent to

$$|\boldsymbol{A} - \boldsymbol{B}\boldsymbol{D}^{-1}\boldsymbol{C}| = 0, \tag{B.12}$$

which is the determinant of a 3×3 matrix. If we take into account only the $q = 0, \pm 1$ multipolar terms, the above equation reduces to $\det \boldsymbol{A} = 0$, and we obtain the well-known low filling fraction approximation. The Δ factor comes from the consideration of the contribution of the terms $\boldsymbol{B}\boldsymbol{D}^{-1}\boldsymbol{C}$, being defined as

$$\Delta = 1 - \boldsymbol{B}\boldsymbol{D}^{-1}\boldsymbol{C}\big|_{11}. \tag{B.13}$$

Note that all the block matrices $\boldsymbol{B}$, $\boldsymbol{C}$ and $\boldsymbol{D}$ are of the form $\hat{T}_q \hat{S}_{qs}$ for $|q|, |s| > 1$, which means that they contain information on the lattice structure, filling fraction and physical properties of the cylinders, but not on the effective speed of sound. By assuming an isotropic lattice (i.e. hexagonal or square) we obtain the following expression for the effective speed of sound

$$\frac{1}{c^*} = \sqrt{\left(\frac{1-f}{B_b} + \frac{f}{B_a}\right)\frac{\rho_a(\Delta + f) + \rho_b(\Delta - f)}{\rho_a(\Delta - f) + \rho_b(\Delta + f)}\rho_b}. \tag{B.14}$$

From which we obtain the effective mass density as

$$\rho^* = \frac{\rho_a(\Delta + f) + \rho_b(\Delta - f)}{\rho_a(\Delta - f) + \rho_b(\Delta + f)}\rho_b. \tag{B.15}$$

Obviously this expression does not depends on frequency since it is obtained in the limit $\omega \to 0$.

In general the low-frequency limit is equivalent to the long-wavelength limit ($\lambda \to \infty$) and, thus, if k_b and k_a are the background and scatterer wavenumbers, respectively, $\omega \to 0$ implies $k_b \to 0$ and $k_a \to 0$. We assume here that $k_b \to 0$, while k_a remains finite. As the scatterer's wave number k_a appears in the secular equation only through the T matrix, the secular equation for a frequency-dependent theory can be easily obtained as

$$\lim_{k_b \to 0} |\boldsymbol{I} - \boldsymbol{T}\boldsymbol{S}| = |\delta_{qs} - \hat{T}_q(k_a)\hat{S}_{qs}| = 0, \tag{B.16}$$

where the limit in

$$\hat{T}_q(k_a) = \lim_{k_b \to 0} \frac{T_q}{k_b^{2|q|}} \tag{B.17}$$

is taken only for the variable k_b but not for k_a, which allows us to define a frequency dependent factor $\Delta = \Delta(k_a)$ through the variable $k_a = \omega/c_a$. The above limit, from the general definition given in (6) after using the asymptotic expressions for the Bessel and Hankel functions, yields

$$\hat{T}_q(k_a) = \lim_{k_b \to 0} \frac{T_q}{k_b^{2|q|}} = \frac{\mathrm{i}\pi R_a^{2q}}{q!(q-1)!2^{2q}} \lim_{k_b \to 0} \frac{q\chi_q/k_b R_a - \rho_b}{q\chi_q/k_b R_a + \rho_b}, \tag{B.18}$$

which is the frequency dependent multipolar contribution to the Δ factor.

References

[1] Liu Z, Zhang X, Mao Y, Zhu Y Y, Yang Z, Chan C T and Sheng P 2000 Locally resonant sonic materials *Science* **289** 1734

[2] Fang N, Xi D, Xu J, Ambati M, Srituravanich W, Sun C and Zhang X 2006 Ultrasonic metamaterials with negative modulus *Nat. Mater.* **5** 452–6

[3] Yang Z, Mei J, Yang M, Chan N H and Sheng P 2008 Membrane-type acoustic metamaterial with negative dynamic mass *Phys. Rev. Lett.* **101** 204301
[4] Ambati M, Fang N, Sun C and Zhang X 2007 Surface resonant states and superlensing in acoustic metamaterials *Phys. Rev.* B **75** 195447
[5] Deng K, Ding Y, He Z, Zhao H, Shi J and Liu Z 2009 Theoretical study of subwavelength imaging by acoustic metamaterial slabs *J. Appl. Phys.* **105** 124909
[6] Yang Z, Dai H M, Chan N H, Ma G C and Sheng P 2010 Acoustic metamaterial panels for sound attenuation in the 50–1000 Hz regime *Appl. Phys. Lett.* **96** 041906
[7] Li J and Chan C T 2004 Double-negative acoustic metamaterial *Phys. Rev.* E **70** 55602
[8] Cheng Y, Xu J Y and Liu X J 2008 One-dimensional structured ultrasonic metamaterials with simultaneously negative dynamic density and modulus *Phys. Rev.* B **77** 45134
[9] Lee S H, Park C M, Seo Y M, Wang Z G and Kim C K 2010 Composite acoustic medium with simultaneously negative density and modulus *Phys. Rev. Lett.* **104** 054301
[10] Veselago V G 1968 The electrodynamics of substances with simultaneously negative values of ϵ and μ *Sov. Phys.—Usp.* **10** 509–14
[11] Pendry J B 2000 Negative refraction makes a perfect lens *Phys. Rev. Lett.* **85** 3966–9
[12] Smith D R, Pendry J B and Wiltshire M C K 2004 Metamaterials and negative refractive index *Science* **305** 788
[13] Shalaev V M 2007 Optical negative-index metamaterials *Nat. Photonics* **1** 41–8
[14] Jacob Z, Alekseyev L V and Narimanov E 2006 Optical hyperlens: far-field imaging beyond the diffraction limit *Opt. Express* **14** 8247–56
[15] Zhang X and Liu Z 2008 Superlenses to overcome the diffraction limit *Nat. Mater.* **7** 435–41
[16] Li J, Fok L, Yin X, Bartal G and Zhang X 2009 Experimental demonstration of an acoustic magnifying hyperlens *Nat. Mater.* **8** 931–4
[17] Cummer S A and Schurig D 2007 One path to acoustic cloaking *New J. Phys.* **9** 45
[18] Cummer S A, Rahm M and Schurig D 2008 Material parameters and vector scaling in transformation acoustics *New J. Phys.* **10** 115025
[19] Chen H and Chan C T 2010 Acoustic cloaking and transformation acoustics *J. Phys. D: Appl. Phys.* **43** 113001
[20] Bin L and Ji-Ping H 2010 Noise shielding using acoustic metamaterials *Commun. Theor. Phys.* **53** 560
[21] Yang T, Cao R F, Luo X D and Ma H R 2010 Acoustic superscatterer and its multilayer realization *Appl. Phys.* A **99** 843–7
[22] Liu Z, Chan C T and Sheng P 2005 Analytic model of phononic crystals with local resonances *Phys. Rev.* B **71** 14103
[23] Ding Y, Liu Z, Qiu C and Shi J 2007 Metamaterial with simultaneously negative bulk modulus and mass density *Phys. Rev. Lett.* **99** 93904
[24] Hu X, Chan C T and Zi J 2005 Two-dimensional sonic crystals with Helmholtz resonators *Phys. Rev.* E **71** 55601
[25] Wang Z G, Lee S H, Kim C K, Park C M, Nahm K and Nikitov S A 2008 Acoustic wave propagation in one-dimensional phononic crystals containing Helmholtz resonators *J. Appl. Phys.* **103** 064907
[26] Hu X, Ho K M, Chan C T and Zi J 2008 Homogenization of acoustic metamaterials of Helmholtz resonators in fluid *Phys. Rev.* B **77** 172301
[27] Wu Y, Li J, Zhang Z Q and Chan C T 2006 Effective medium theory for magnetodielectric composites: beyond the long-wavelength limit *Phys. Rev.* B **74** 085111
[28] Peng L, Ran L, Chen H, Zhang H, Kong J A and Grzegorczyk T M 2007 Experimental observation of left-handed behavior in an array of standard dielectric resonators *Phys. Rev. Lett.* **98** 157403
[29] Schuller J A, Zia R, Taubner T and Brongersma M L 2007 Dielectric metamaterials based on electric and magnetic resonances of silicon carbide particles *Phys. Rev. Lett.* **99** 107401
[30] Vynck K, Felbacq D, Centeno E, Căbuz A I, Cassagne D and Guizal B 2009 All-dielectric rod-type metamaterials at optical frequencies *Phys. Rev. Lett.* **102** 133901

[31] Chern R L and Liu X X 2010 Effective parameters and quasi-static resonances for periodic arrays of dielectric spheres *J. Opt. Soc. Am.* B **27** 488–97
[32] Pendry J B, Holden A J, Robbins D J and Stewart W J 1999 Magnetism from conductors and enhanced nonlinear phenomena *IEEE Trans. Microw. Theory Tech.* **47** 2075–84
[33] Sarychev A K, McPhedran R C and Shalaev V M 2000 Electrodynamics of metal–dielectric composites and electromagnetic crystals *Phys. Rev.* B **62** 8531
[34] Hu X, Chan C T, Zi J, Li M and Ho K M 2006 Diamagnetic response of metallic photonic crystals at infrared and visible frequencies *Phys. Rev. Lett.* **96** 223901
[35] Wu Y, Lai Y and Zhang Z Q 2007 Effective medium theory for elastic metamaterials in two dimensions *Phys. Rev.* B **76** 205313
[36] Torrent D, Hkansson A, Cervera F and Sánchez-Dehesa J 2006 Homogenization of two-dimensional clusters of rigid rods in air *Phys. Rev. Lett.* **96** 204302
[37] Torrent D and Sánchez-Dehesa J 2006 Effective parameters of clusters of cylinders embedded in a nonviscous fluid or gas *Phys. Rev.* B **74** 224305
[38] Torrent D and Sánchez-Dehesa J 2008 Anisotropic mass density by two-dimensional acoustic metamaterials *New J. Phys.* **10** 023004
[39] Morse P M C and Ingard K U 1986 *Theoretical Acoustics* (Princeton, NJ: Princeton University Press)
[40] Abramowitz M and Stegun I A 1964 *Handbook of Mathematical Functions with Formulas, Graphs and Mathematical Tables* (New York: Dover)
[41] Berryman J G 1980 Long-wavelength propagation in composite elastic media. I. Spherical inclusions *J. Acoust. Soc. Am.* **68** 1809
[42] O'Brien S and Pendry J B 2002 Photonic band-gap effects and magnetic activity in dielectric composites *J. Phys.: Condens. Matter* **14** 4035
[43] Krokhin A and Reyes E 2004 Homogenization of magnetodielectric photonic crystals *Phys. Rev. Lett.* **93** 023904
[44] Felbacq D and Bouchitté G 2005 Theory of mesoscopic magnetism in photonic crystals *Phys. Rev. Lett.* **94** 183902
[45] Reyes E, Krokhin A A and Roberts J 2005 Effective dielectric constants of photonic crystal of aligned anisotropic cylinders and the optical response of a periodic array of carbon nanotubes *Phys. Rev.* B **72** 155118
[46] Torrent D and Sánchez-Dehesa J 2009 Radial wave crystals: radially periodic structures from anisotropic metamaterials for engineering acoustic or electromagnetic waves *Phys. Rev. Lett.* **103** 64301
[47] Spiousas I, Torrent D and Sánchez-Dehesa J 2011 Experimental realization of broadband tunable resonators based on anisotropic metafluids *Appl. Phys. Lett.* **98** 244102
[48] Torrent D and Sánchez-Dehesa J 2010 Anisotropic mass density by radially periodic fluid structures *Phys. Rev. Lett.* **105** 174301
[49] Torrent D and Sánchez-Dehesa J 2007 Acoustic metamaterials for new two-dimensional sonic devices *New J. Phys.* **9** 323
[50] Pendry J B and Li J 2008 An acoustic metafluid: realizing a broadband acoustic cloak *New J. Phys.* **10** 115032
[51] Norris A N 2009 Acoustic metafluids *J. Acoust. Soc. Am.* **125** 839